

Laser Processing of Intraocular Lenses

Alexandra Sinani ^{1,2}, Dimitrios Palles ¹ , Constantinos Bacharis ¹, Dionysios Mouzakis ³ , Maria Kandyla ¹
and Christos Riziotis ^{1,4,*} 

¹ Theoretical and Physical Chemistry Institute, National Hellenic Research Foundation, 11635 Athens, Greece; asinani@eie.gr (A.S.); dpalles@eie.gr (D.P.); cbacharis@yahoo.gr (C.B.); kandyla@eie.gr (M.K.)

² Department of Informatics and Computer Engineering, University of West Attica, Egaleo, 12243 Athens, Greece

³ Laboratory of Mechanics, Department of Military Sciences, Hellenic Army Academy, 16673 Athens, Greece; dmouzakis@eie.gr

⁴ Defence & Security Research Institute, University of Nicosia, Nicosia CY-2417, Cyprus

* Correspondence: riziotis@eie.gr; Tel.: +30-2107273887

Abstract: Polymeric Intraocular lenses (IOLs) are vital for restoring vision following cataract surgery and for correcting refractive errors. Despite technological and medical advancements, challenges persist in achieving optimal vision and preventing complications. Surface modifications aim to mitigate the risk of posterior capsule opacification (PCO), while pre-operative measurements aid in selecting suitable IOLs. However, individualized solutions are lacking and there is a clear demand for the development of fully customized IOL surfaces. We employ laser micromachining technology for precise modifications via ablation on PMMA and acrylic IOLs, using femtosecond (fs), nanosecond (ns), and diode continuous wave (CW) lasers, at wavelengths ranging from near-ultraviolet to infrared. Characterization reveals controlled ablation patterning, achieving feature sizes from as small as 400 nm to several micrometers. Regular and confocal micro-Raman spectroscopy revealed alterations of the IOL materials' structural integrity for some patterning cases, thus affecting the optical properties, while these can be minimized by the proper selection of micromachining conditions. The results suggest the feasibility of accurate IOL patterning, which could offer personalized vision correction solutions, based on relevant corneal wavefront data, thus surpassing standard lenses, marking a significant advancement in cataract surgery outcomes.



Citation: Sinani, A.; Palles, D.; Bacharis, C.; Mouzakis, D.; Kandyla, M.; Riziotis, C. Laser Processing of Intraocular Lenses. *Appl. Sci.* **2024**, *14*, 6071. <https://doi.org/10.3390/app14146071>

Academic Editor: Mario Gai

Received: 5 June 2024

Revised: 6 July 2024

Accepted: 10 July 2024

Published: 11 July 2024



Copyright: © 2024 by the authors. Licensee MDPI, Basel, Switzerland. This article is an open access article distributed under the terms and conditions of the Creative Commons Attribution (CC BY) license (<https://creativecommons.org/licenses/by/4.0/>).

Keywords: intraocular lens; PMMA; acrylic; laser ablation; femtosecond laser; nanosecond laser; continuous wave laser; diode laser; Raman spectroscopy

1. Introduction

Intraocular lenses (IOLs) are artificial lenses that play a crucial role in restoring vision for individual patients undergoing cataract surgery or seeking correction for refractive errors such as myopia, hyperopia, astigmatism, and presbyopia. Cataracts are a common eye condition that causes the eye's natural lens to become cloudy, leading to blurred vision [1]. During cataract surgery, the natural crystalline lens is broken up and removed through small incisions, followed by the insertion of an IOL into the capsular bag. IOLs are typically made from materials such as acrylic, polymethyl methacrylate (PMMA), or silicone, adhering to strict FDA or similar biocompatibility standards [2,3]. Some IOLs may also have special coatings to reduce the risk of complications [4,5].

Following cataract surgery, patients often face challenges in choosing between distance and near vision correction, leading to reliance on spectacles [6,7]. Although toric [8], multifocal [9], and accommodative IOLs have been developed to address these challenges, achieving perfect vision remains intangible despite advancements in IOL technology. Another common issue following cataract surgery is the posterior capsule opacification (PCO), also known as a secondary cataract. While the conventional treatment for PCO involves

Nd:YAG laser capsulotomy, it is associated with complications like IOL damage, macular edema, increased intraocular pressure, and a higher risk of retinal detachment [10,11]. As an alternative to treatment, extensive research has explored the role of IOL surface modifications in reducing PCO incidence. Surface-modified IOLs aim to prevent Lens Epithelial Cell (LEC) migration to the center of the posterior capsule and enhance biocompatibility [12]. While pre-operative measurement of corneal spherical aberration aids in selecting suitable IOLs [13], even the best available lens may not fully meet each patient's unique needs. To address this, the focus is on developing IOLs that integrate comprehensive corneal wavefront data, enabling the creation of fully customized IOL surfaces tailored to individual patient requirements, thus offering personalized vision correction solutions beyond standard lenses.

IOLs are typically manufactured by industrial injection molding machines based on specific designs for curvature, thickness, and other optical characteristics. The mass production is efficient; however, there is a clear and strong demand for the on-site rapid customization of IOLs based on relevant corneal wave front data acquired by ophthalmologists at the eye-surgery clinic. Such an approach for IOLs rapid customization is feasible by laser patterning, where further to the low-cost implementation for efficient usage at eye-surgery clinics, a few requirements need to be satisfied such as capability of accurate patterning in the range of a submicron to a few micrometers, minimum optical roughness, and no degradation of IOLs in terms of optical, structural, and compositional characteristics. However, the tolerances in the degradation of optical characteristics have not been fully quantified yet by the ophthalmic surgery community.

Although the laser patterning of IOLs is under study by a limited number of research groups during almost the past 20 years, an adequate number of systematic and extended studies with conclusive results on IOL patterning has not yet been achieved. One reason could be that scattered studies internationally are based on available laser sources in various research labs without the capability of a direct comparison, or optimal laser selection, in the same study. Another reason is that commercially available IOLs vary in terms of materials (PMMA, silicone, acrylic, hydrophobic acrylic, etc.) and can have very different characteristics and polymer compositions, not always publicly disclosed, making very difficult if not impossible the standardization of the IOL study under various laser processing studies. Therefore, there is a clear need for further studies with new micromachining approaches as there is a considerable gap and a long way to the successful laser-based customization of IOLs.

Laser technology has been widely utilized in various technological, industrial, and medical fields for material processing purposes over the course of many years [14–17]. It finds applications in ablating, drilling, cutting, and other material modifications achieved by focusing concentrated laser energy onto the target material. The advantages of laser processing, such as reduced heat-affected zones, speed, versatility, and environmental considerations, make it stand out among alternative methods as it also provides rapid prototyping and customizable solutions. The available lasers cover a spectrum of pulse durations, from continuous wave (CW) operation to nanosecond (ns), picosecond (ps), and femtosecond (fs) pulses, and also at various wavelengths from ultraviolet to the infrared band. Many studies have been performed into the physics of ultrashort pulse laser–matter interaction, emphasizing the differences in ablation mechanisms between short and ultrashort pulses [18–21]. The utilization of laser ablation by femtosecond lasers has been previously studied as an approach for patterning and shaping IOLs [22–24]. The primary goal was to provide ophthalmologists with a tool for tailoring IOL patterns to suit the specific needs of individual patients using laser technology.

In this work, the laser ablation process was employed to create processed areas on the curved surface of commercially available IOLs. Two types of IOLs were considered: non-flexible PMMA lenses and flexible acrylic lenses. The primary objective is to produce the uniform and consistent modification of the IOL's surface. By creating a homogeneous processed area, the IOLs are more likely to exhibit consistent optical properties and char-

acteristics, which is important for achieving predictable and reliable visual functionality for patients who undergo cataract surgery and have these IOLs implanted. We employed three types of lasers, a femtosecond laser, a nanosecond laser, and a continuous wave diode laser, with very different characteristics, covering a wide range of laser sources in this study. Specifically, the femtosecond laser system emitted 370 fs pulses and operated at a wavelength of 1064 nm. The nanosecond laser system operated at 355 nm with a 5 ns pulse duration. The CW diode laser operated at a wavelength of 405 nm. Firstly, ablated areas were systematically produced on the surface of both IOLs using the femtosecond laser. Additionally, a detailed study was conducted to determine the optimal laser parameters for producing spot patterns with desired characteristics, involving both the CW diode and nanosecond laser. Overall, the experiments aimed at understanding the effects of the laser ablation of various types of lasers on different IOLs and to optimize the laser parameters for achieving uniform and consistent modifications on the IOL surfaces, thus identifying suitable laser patterning approaches potentially compatible with highly accurate IOL modification needed. This study was also supported with Raman spectroscopy for the identification of possible alterations of optical and structural properties of laser-processed IOLs, which is an important element for their usability.

2. Materials and Methods

2.1. IOLs

Two kinds of IOLs were used for laser processing. First, the PMMA lens (Spheric IOL, model: Balance, Hanita lenses, Hanita, Israel) is constructed from polymethyl methacrylate with refractive index $n = 1.49$. Second, the flexible acrylic lens (Aspheric IOL, model: SA60WF, Acrysof[®], Alcon Inc., Geneva, Switzerland) is composed of a hydrophobic Acrylate/Methacrylate Copolymer material with refractive index $n = 1.55$. Both of these IOLs are designed for posterior chamber implantation, include a UV radiation filter, have a lens power of +21.5, an optic diameter of 6 mm, and an overall length of 12.5 mm and 13 mm, respectively.

2.2. IOL Characterization

Optical transmission spectra were obtained by means of a UV-VIS-NIR spectrophotometer (C-7200, PEAK Instruments, Shanghai, China). The surface morphology of the laser-patterned samples was examined via a JSM-7600F Schottky Field Emission Scanning Electron Microscope by JEOL (Tokyo, Japan) operating at 10 kV to 15 kV. Various magnifications were employed during the SEM analysis, ranging from $\times 100$ to $\times 10,000$. The samples were attached to the sample holder with conductive copper tape and coated with gold/platinum by using the SC7620 Mini Sputter Coater/Glow Discharge System by Quorum (East Sussex, UK), to enhance their conductivity and reduce charging effects during imaging. Moreover, optical images of the patterned areas in top view were obtained via an optical microscope (ADL 601 P, BRESSER Science, Rhede, Germany), equipped with a micro-camera. The surface topography analysis was performed with an Alpha-Step IQ surface profilometer (KLA-Tencor, Milpitas, CA, USA), a stylus-based step profiler. The assessment of microstructural and chemical modifications in laser-treated areas was conducted using regular and confocal micro-Raman spectroscopy (Renishaw, inVia Reflex Raman microscope, Wotton-under-Edge, UK). The spectra were measured using an argon ion (Ar^+) laser for excitation at 514.5 nm. Both a $\times 20$ ($NA: 0.40$) and a $\times 100$ ($NA: 0.85$) objective lens were employed, offering a nominal spatial resolution ($0.61 * \lambda / NA$) of ca. 785 nm and 370 nm, respectively.

2.3. Femtosecond Laser Micromachining Setup

An ultrashort fiber-based laser system was employed (HE-1060-1 uJ-fs, Fianium, Southampton, UK), which emits laser pulses with a duration of 370 fs at a wavelength of 1064 nm. The laser has maximum pulse energy of 1 μJ , and a variable repetition rate up to 1 MHz. The power values were monitored using a thermal power sensor (S302C,

Thorlabs, Newton, NJ, USA). The laser beam was focused onto the IOL surface using a $\times 20$ achromatic standard objective lens with a numerical aperture (NA) of 0.4 (Edmund Optics, Barrington, IL, USA). The beam spot size was $\sim 3.6 \mu\text{m}$ as calculated by the equation

$$d = 4M^2\lambda f / \pi D_0, \quad (1)$$

where M^2 is the beam quality (1.2), λ is the laser wavelength, f is the focal length of the lens (8.3 mm), and D_0 is the diameter of the laser beam before the lens (3.8 mm). The IOL samples were placed on X - Y motorized linear stages with a nominal resolution of 1 nm (Smaract, CLS-92152, Oldenburg, Germany), allowing for precise movement and positioning (Figure 1). This setup was designed to facilitate controlled and precise laser-induced modifications on the IOLs' surface. A CMOS monochrome camera (Teledyne Dalsa, Genie Nano M640, Waterloo, ON, Canada) was used for imaging and determining the laser focus position on the IOLs.

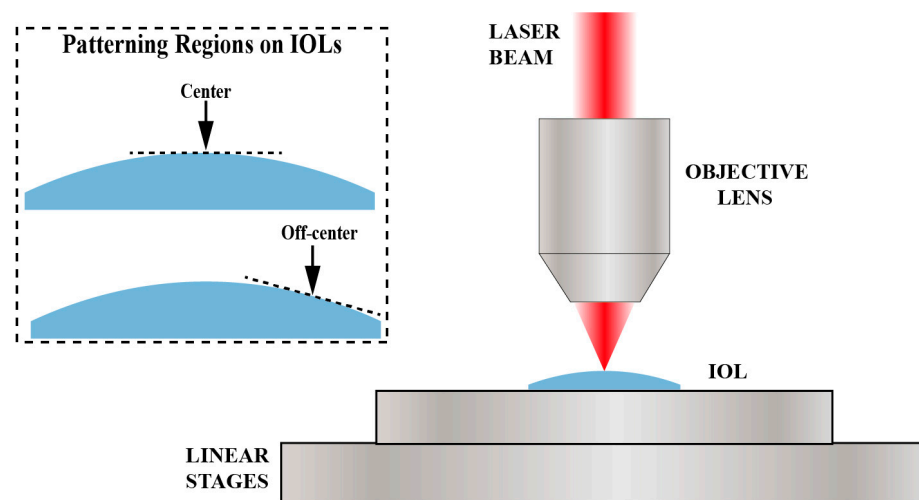


Figure 1. Schematic representation of laser ablation on IOLs and associated patterning regions.

2.4. Nanosecond Laser Setup

A pulsed Q-switched Nd:YAG laser system was employed (Nano S 130-10, Litron Lasers, Rugby, UK), operating at the third harmonic wavelength of 355 nm, with a pulse duration of 5 ns and a repetition rate of 10 Hz, and operated at a stable pulse energy of 7.2 mJ. The laser beam was focused utilizing a plano-convex lens with a focal length of 200 mm, resulting in an incident fluence of 1.1 J/cm^2 . As illustrated in Figure 1, the samples were positioned on a motorized platform, enabling movement along both the X - Y axes.

2.5. CW Diode Laser Micromachining Setup

A low-cost CW diode laser was employed (4PICO, HSLU) with a wavelength of 405 nm, producing a collimated laser beam with maximum power at 36 mW. The optical power of the laser was measured with a photodiode power sensor (Thorlabs, S120C). The laser operated either with an external trigger mode for multi-shot experiments or a continuous mode for line ablation. The beam was focused onto the IOL surface using a high-magnification objective lens with $NA = 0.90$ (Corning Tropel, Glendale, Arizona) and the beam spot size was approximately 300 nm. The IOL samples were placed vertically on the X - Y motorized linear stages (Smaract, CLS-92152, Oldenburg, Germany) and a CMOS monochrome camera (Genie Nano M2020, Teledyne Dalsa, Waterloo, ON, Canada) was used for maintaining precise focusing during the experiments. Due to the specific optical arrangement, the sample in the diode writing setup was moving only in one axial direction in this setup.

3. Results

3.1. Optical Properties

Optical transmission spectra were measured between 300 nm and 1000 nm for the two kinds of IOLs employed here (Figure 2). We observe an absorption cut-off wavelength at 400 nm for both lenses. Therefore, the CW laser with a wavelength of 405 nm and the 355 nm of the nanosecond laser are strongly absorbed by the lenses. Even though the wavelength of the femtosecond laser (1064 nm) falls within the transparent regime of these lenses, tight focusing of the laser beam, and multiphoton absorption in the fs laser case, achieves efficient laser patterning on the surface of the IOLs, as demonstrated in the following sections.

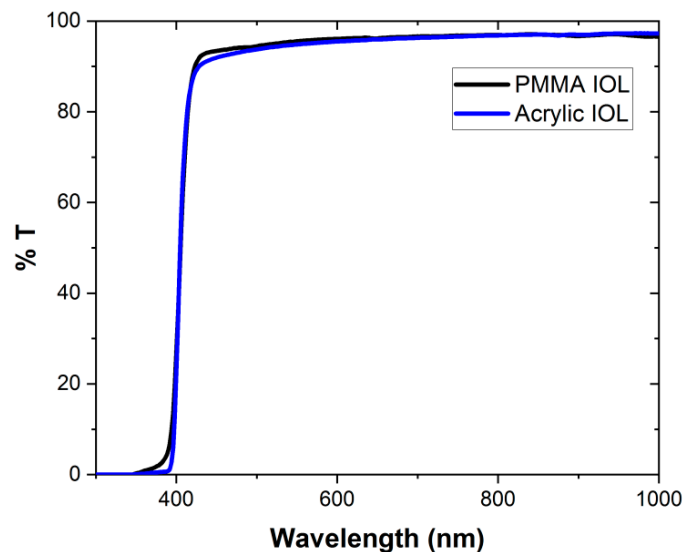


Figure 2. Optical transmission spectra for PMMA and acrylic IOLs.

3.2. Fabrication and Characterization of Femtosecond Laser-Induced Micro-Patterns

A homogenous ablated area was formed on the central region of the PMMA IOL, as shown in Figure 3a,b, following irradiation with a pulse energy of 0.8 μJ and repetition rate of 100 kHz. Additionally, another ablated area was formed on the off-centered, curved side of the lens, as shown in Figure 3c,d. These areas covered a rectangular area of 100 μm in width and 200 μm in length and were created with a continuous scanning process without refocusing the objective lens. The lateral separation between each parallel scan was set at 4 μm , a value that approaches the theoretical beam spot size of the lens (3.6 μm). The intention was to achieve an effective overlap between parallel scans for a uniformly modified surface. For each line scan, the translation was set at 200 μm and the scanning speed at 10 $\mu\text{m}/\text{s}$. The ablation process on the PMMA IOLs results in the formation of a symmetrical region around the focal spot, overall displaying the characteristic roughness and porosity of a PMMA laser-ablated surface [25,26]. The laser processing parameters were selected in order to prevent excessive damage on the surface of the PMMA IOL.

It can be observed that when patterning at the off-centered, curved side of the IOL, due to varying focus conditions, there are residual threads of removed material, leading to incomplete ablation and increased surface roughness. However, our findings highlight the critical influence of precise focus conditions on the patterning mechanism and the consistency of the ablation procedure. By further optimizing the linear patterns' overlap and the writing depth, the surface uniformity and the roughness of the patterned area could be further improved where needed in real applications.

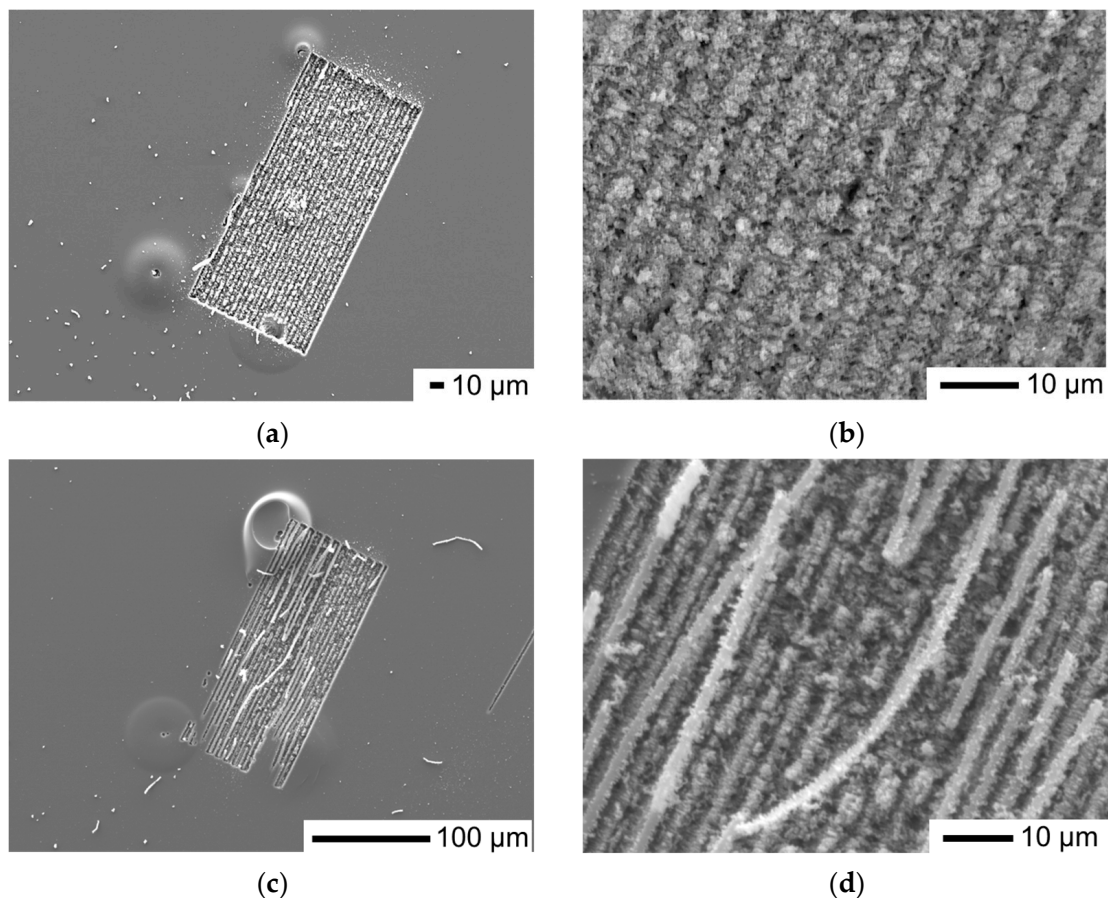


Figure 3. SEM images (top view) of the ablated areas. (a,b) At the center of the PMMA IOL; (c,d) on the off-centered, curved side of the PMMA IOL.

On the off-centered, curved side of the acrylic IOL, we again created a 100 μm in width and 200 μm in length rectangular area using exactly the same exposure conditions as those employed for the PMMA IOL. This process results in the creation of structured regions, as illustrated in Figure 4a–c, which portray the ablated area at various magnifications. The SEM analysis reveals several notable features such as an expanded width in a single line scan, as presented in Figure 4d; the presence of molten material; and the formation of micro-cavities. The observed micron-sized cavities likely result from gas release during the thermal degradation of the acrylic material. These findings strongly indicate localized thermal modification in the patterned area, representative of a photo-thermal ablation process. Although heat accumulation effects with femtosecond lasers typically manifest for repetition rates higher than 200 kHz or even 1 MHz [27,28], the response depends on the thermal properties of the target material. Properties including thermal diffusivity, melting point, and heat capacity play a fundamental role in determining its response to the intense heat generated during laser ablation. For example, the thermal diffusivity of PMMA and other acrylic polymers can be influenced by the molecular weight or the presence of additives in the polymer [29]. These factors can significantly affect the ablation process, potentially altering the material's behavior under laser exposure.

The peak laser fluence is determined, considering a Gaussian beam, using the equation

$$F = E_p / \pi(d/2)^2, \quad (2)$$

where E_p represents the pulse energy set at 0.8 μJ and d is the focused beam diameter. The peak fluence used for the micromachined areas was 8 J/cm^2 . This value exceeds the ablation threshold for both PMMA and acrylic materials. We also determine the effective

number of pulses delivered per surface area, calculated as 40×10^3 for both IOLs, utilizing the formula

$$N = RR \times d/s, \quad (3)$$

where RR represents the pulse repetition rate, d is the focused beam diameter, and s is the translating speed of the stage.

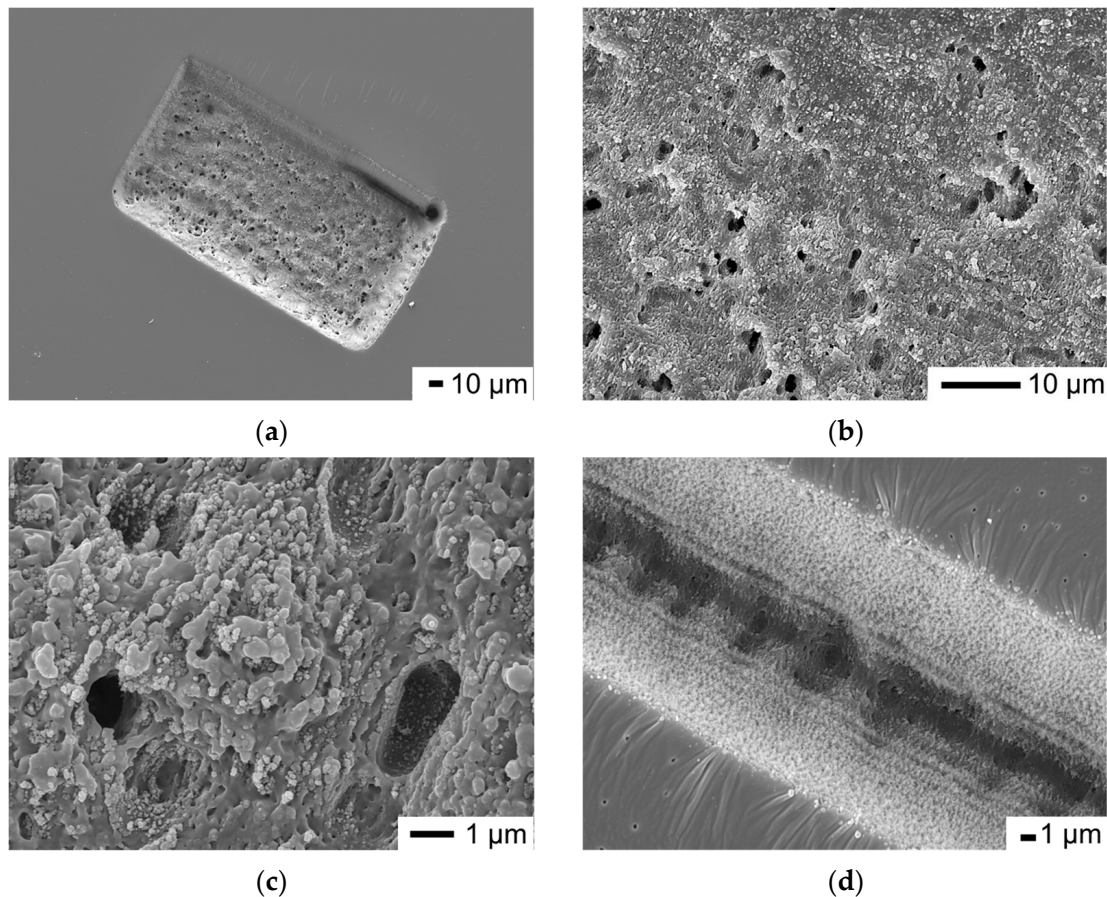


Figure 4. SEM images (top view) of the ablated areas on the off-centered, curved side of the acrylic IOL. (a–c) Ablated area with different magnifications; (d) ablated line scan.

Following irradiation by the femtosecond laser, we performed depth measurements with the surface profilometer, along the short dimension of the ablated areas (100 μm in width), to evaluate the material modification and the precision in the laser ablation process. As indicated in Figure 5, the ablation depth for the PMMA IOL ranges from 3 to 3.5 μm in the area created at the center of the lens (blue line) and from 1 to 3 μm in the area located on the off-centered, curved side of the lens (red line). In contrast, for the acrylic IOL, the measurement of the modified area located on the off-centered, curved side of the lens (black line) exhibits a deeper ablation depth of 20 to 30 μm , as shown in Figure 5. In the off-centered modified regions of the lenses, the surface exhibits non-uniform modification depth, indicating variations probably due to the different distance from the beam focus and the absence of refocusing during the irradiation process.

Further investigation into irradiation parameters with the femtosecond laser revealed that employing higher repetition rates, such as 1 MHz, in combination with the different materials under examination, resulted in a significant increase in ablation depth. This was evidenced by the observation of 50 μm deep and 50 μm wide ablation spots observed on PMMA IOLs, as shown in the measurements obtained with the surface profilometer in Figure 6. This increase can be attributed to the higher energy delivered to the target material per unit time, resulting in more substantial material removal per laser pulse or over a given

time. The higher energy levels or repetition rates impart greater momentum to the laser-induced plasma, leading to increased material ejection and, consequently, deeper ablation depths. Additionally, the scanning speed is another parameter affecting the ablation depth. This observation underscores the significant influence of laser writing parameters [30] on the material processing characteristics, particularly in the context of the laser ablation of IOLs for applications such as surface modification. The further exploration of different irradiation parameters could potentially lead to achieving similar modifications on acrylic IOL to those achieved on PMMA IOL.

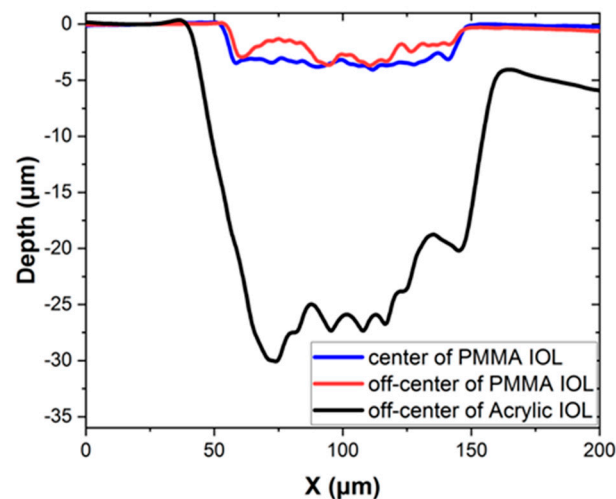


Figure 5. Indicative depth measurements of the ablated areas after irradiation with the femtosecond laser. PMMA IOL: two ablated areas, at the center (blue line) and off-center (red line) of the lens. Acrylic IOL: one ablated area off-center (black line) of the lens.

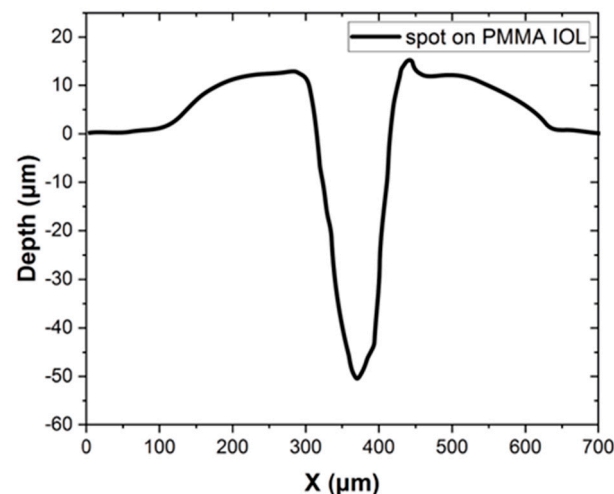


Figure 6. Depth measurement of an abated spot on PMMA IOL irradiated with the femtosecond laser at 1 MHz.

The above findings suggest that the employed infrared femtosecond laser can be efficiently used for patterning in both PMMA and acrylic IOLs' surface with very good repeatability and resolution due to the consistent response of the material. Various femtosecond lasers have been employed in the past. For example, in [22], an 800 nm fs laser with much higher pulse energy up to 200 μJ , but with a low repetition rate of 5 kHz, was employed for writing linear structures with depths up to 5 μm . Also, in [23], a femtosecond laser at 520 nm with much lower pulse energy of 1 nJ was employed for IOL but with discontinuous line patterning due to thermal effects attributed to the very high repetition rate of 63 MHz.

In general, two distinct regimes of femtosecond laser writing or micromachining can be identified based on the pulse period relative to the time required for heat to diffuse away from the focal volume. The low-frequency regime with high-energy pulses involves material modification by individual or low-frequency pulses, while the high-frequency regime with low-energy pulses involves cumulative thermal effects. These two distinct regimes are essentially represented in the aforementioned cases in references [22,23] previously discussed. The heat diffusion time (τ_{heat}) of the absorption volume in the material under investigation is related to the thermal diffusivity (D) and the characteristic diffusion length (L), through the following equation [31]:

$$\tau_{\text{heat}} = L^2/D \quad (4)$$

The transition between these two regimes occurs at laser repetition frequencies defined as the inverse of τ_{heat} . In a previous work [28] for the case of laser writing and patterning in glasses, an intermediate regime of optimum laser writing and patterning conditions was identified, by a typical fiber Yb-based laser emitting at 1030 nm, with pulse energy $\sim 1 \mu\text{J}$, ~ 300 fs pulse duration, and repetition rate at ~ 1 MHz. This laser provided by far the best laser writing performance in glass, enabling fast processing with eliminated heat accumulation effects, and resulted in uniform structures, as in typical glasses, the heat diffusion time is $\tau_{\text{heat}} \sim 1 \mu\text{s}$ and the transition should occur at around 1 MHz [28]. Our results indicate that an analogous behavior was observed in the patterning of polymer IOLs. For glasses, the thermal diffusivity is around $D \sim 0.6 \text{ mm}^2/\text{s}$ while for PMMA, it is roughly $D \sim 0.1 \text{ mm}^2/\text{s}$ [29]. Therefore, the τ_{heat} is estimated to be much slower (by a factor of ~ 6) in polymers, compared to glasses, and the expected transition frequency should be correspondingly lower. This is in agreement with our findings, as the femtosecond system we employed (with the capability of tunable repetition rate between single pulse and 1 MHz) operated in this intermediate regime (100 kHz), which has been demonstrated to offer superior micromachining characteristics, providing enhanced patterning capabilities and flexibility. However, the exact identification of the intermediate regime was not possible as it depends drastically on characteristics of polymers like the molecular weight, which was not known for the commercially used IOLs.

3.3. Nanosecond Laser Ablation of Acrylic IOLs

We conducted experiments involving the creation of ablated spots or craters on the surface of acrylic IOLs using the nanosecond laser with different exposure times and pulse energy at 7.2 mJ. This allows us to observe how the duration of exposure affects the dimensions and characteristics of the resulting craters. The SEM images of the ablated spots are shown in Figure 7.

For the 30 s exposure, the crater dimensions are measured as $630 \times 440 \mu\text{m}$ with resolidified debris around the edges (Figure 7a). With an increase in exposure time to 1 min, the crater dimensions expand to $880 \times 650 \mu\text{m}$ (Figure 7b). Notably, in the case of the 1 min exposure, we observe a dome-like feature above the crater, which indicates a micro-explosion inside the bulk or beneath the surface of the IOL. This suggests that prolonged exposure to the nanosecond laser results in significant material disruption within the IOL. Subsequently, for the 6 min exposure, the crater dimensions further increase to $1030 \times 740 \mu\text{m}$, and the ablation results in a well-formed crater but the ablation depth exceeds the IOL thickness, which is $\sim 500 \mu\text{m}$, penetrating the back side of the IOL (Figure 7c). The elliptical pattern observed as evidenced by the dimensions of the ablated spots indicates the spatial characteristics of the corresponding laser beam during the ablation process. This variation in crater dimensions and characteristics highlights the sensitivity of the nanosecond laser ablation process to exposure time, where despite being slow and relatively controllable in the regime of a several-minute processing duration, with longer exposures it can lead to more extensive material removal and potential structural changes within the IOL.

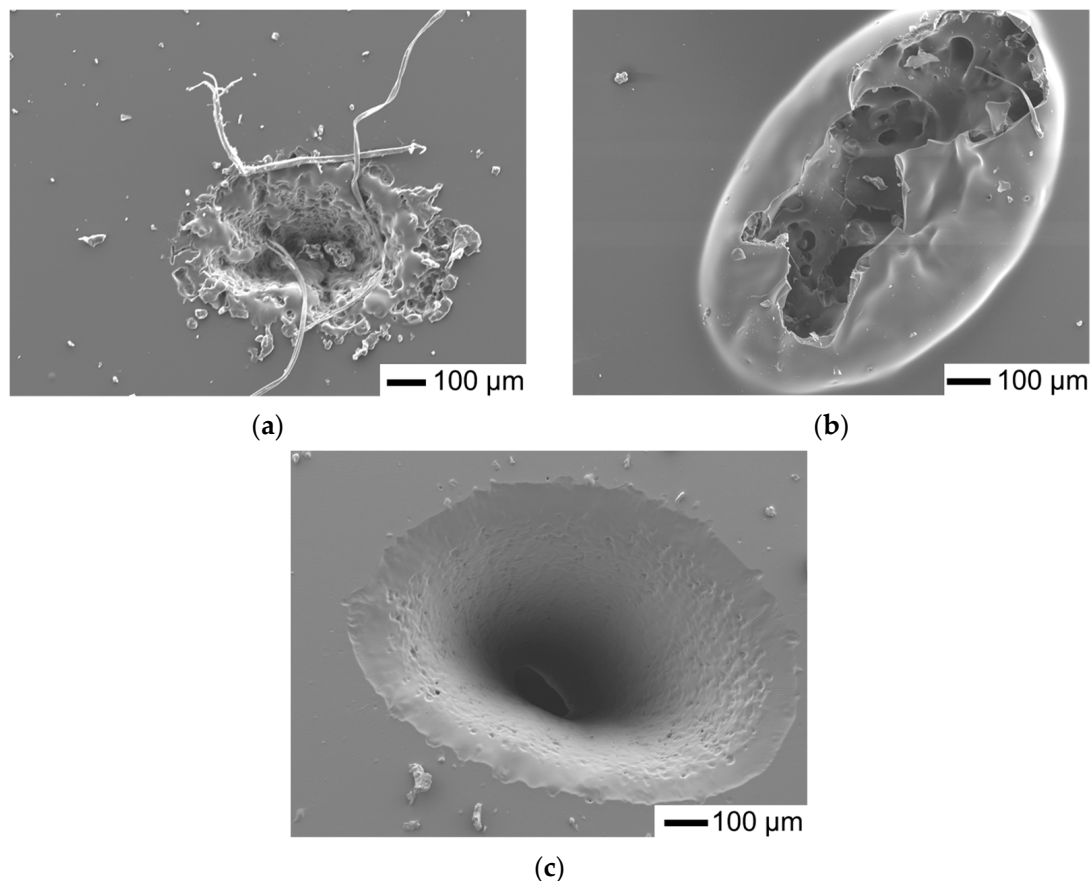


Figure 7. SEM images (top view) of ablated spots on the acrylic IOL after irradiation with the ns laser for (a) 30 s; (b) 1 min; (c) 6 min.

Comparing these results with those obtained with the femtosecond laser reveals interesting insights. The femtosecond laser ablation process typically yields finer and more precise ablation patterns due to its ultrafast pulse duration, high peak power, and suppressed thermal effects [32,33]. In contrast, nanosecond laser ablation tends to result in larger and less controlled ablation areas, as observed in these experiments. Additionally, the presence of an explosion-like patterning of material under the surface, as seen in the 1 min exposure, highlights a distinct effect of nanosecond laser ablation, attributed to increased thermal effects, not typically observed with femtosecond lasers.

3.4. CW Diode Laser Patterns

A series of patterning experiments were conducted also with the CW laser at 405 nm as it provides very different laser characteristics compared to previous cases. However, due to a specific optical arrangement and horizontal exposure configuration of the writing system, the pattern generation was limited to a single line direction or stationary spot exposure. Specifically, for the acrylic IOLs, the translation distance range was set to 900 μm , with a scanning speed of 1 $\mu\text{m}/\text{s}$, and an order of magnitude smaller than the femtosecond setup. The power delivered on the surface was 10 mW, resulting in an intensity of 14 MW/cm^2 . The final ablated line is 450 μm in length and 3.5 μm in width, as shown in Figure 8a, mainly influenced by the IOL curvature and limited depth of focus of the objective lens. The depth of ablation for the line, as measured with the surface profilometer, is approximately 400 nm as shown in Figure 8b. Considering the objective lens spot size of 300 nm and the observed line width of 3.5 μm , thermal effects likely play a significant role in this process.

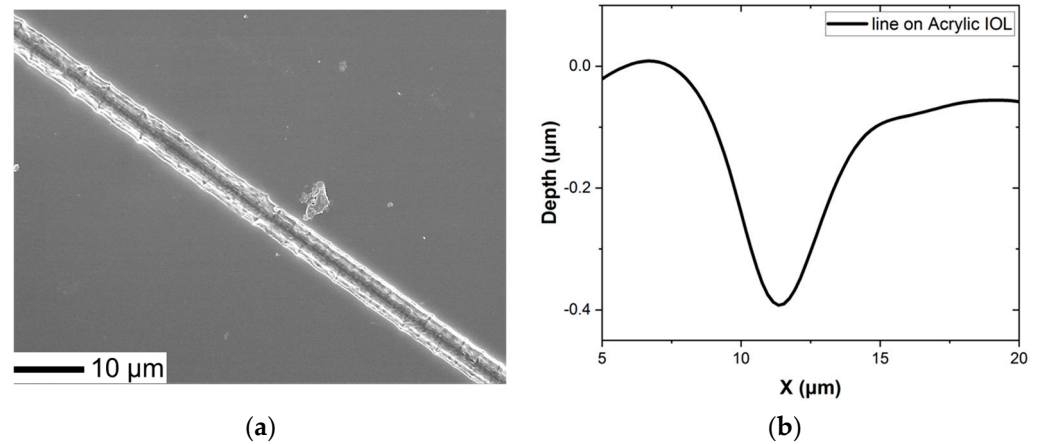


Figure 8. (a) An SEM image (top view) of the ablated area on the acrylic IOL after irradiation with the CW, 405 nm laser; (b) depth measurement of the ablated line.

Additionally, we conducted experiments exposing a single point to varying durations of 1 s, 2 s, 5 s, and 10 s. These exposures resulted in ablated spots with crater dimensions of 0.6 μm , 0.8 μm , 1.2 μm , and 2.1 μm , respectively, as illustrated in Figure 9a. The experimental results, showcasing a gradual increase in the ablated area, indicate a linear correlation between exposure time and the size of the ablated spot, as indicated in Figure 9b, emphasizing the temporal dependence of the laser ablation process on the IOLs.

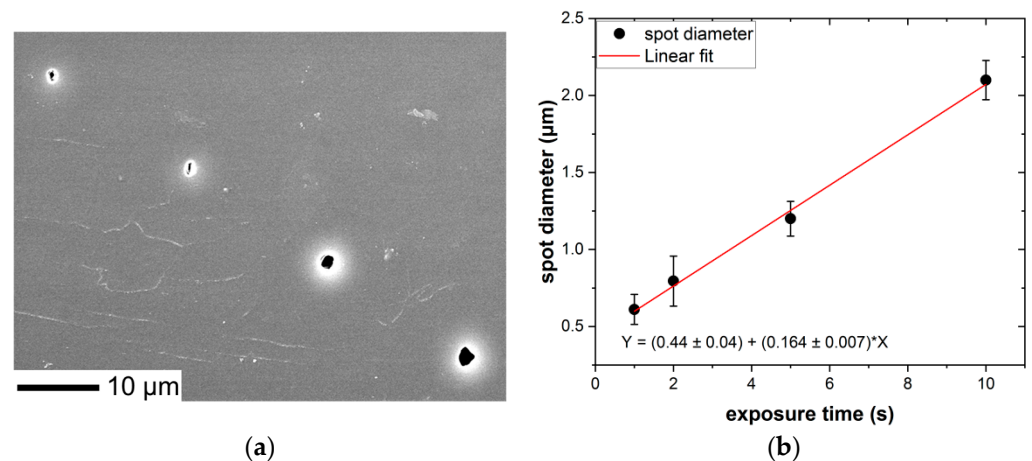


Figure 9. (a) An SEM image (top view) of the ablated spots on the acrylic IOL after irradiation with the CW, 405 nm laser, with exposure times 1 s, 2 s, 5 s, and 10 s from left to right; (b) the correlation of ablated spots' diameters and exposure time.

The use of the 405 nm CW diode laser for patterning the PMMA IOL demonstrates its capability for precise and controlled ablation, despite the limited patterning data we have obtained in this study. However, in several patterning experiments, it was noticed that the exposed area was discontinuously patterned. This phenomenon can be partially attributed to the low exposure power for this material and the non-adaptive focusing of the beam when transferred in a non-uniform IOL with varying curvatures. However, it can also be attributed to the fact that the processing occurs in the thermal processing regime where the accumulation of continuous laser radiation or discrete multiple pulses lead to an increase in local temperature and modification of polymers' properties. The same phenomenon has been described in femtosecond laser patterning in [23]. Such discontinuous patterns are shown in the optical microscope image in Figure 10. Due also to technical issues with the gold post-sputter coating process before the SEM characterization, it was difficult to provide SEM images for the in-detail visualization of those discontinuous patterns. It should be stressed that this is the first demonstration of successful patterning of IOLs by

a compact and low-power CW diode laser, which provides a considerable potential for low-cost IOL patterning; however, further studies are required to address these challenges and optimize the process.

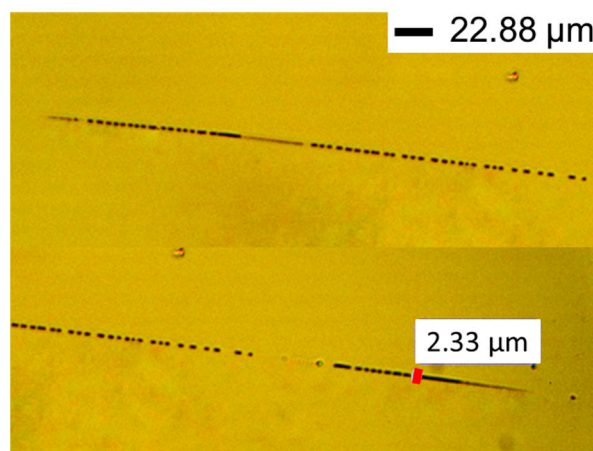


Figure 10. An optical microscope image of the ablated line created on the PMMA lens with the CW 405 nm laser.

The process with the CW laser differs significantly compared to the other two lasers, due to the differences in wavelength and energy delivery mechanism or the materials' laser-induced modification processes. While the nanosecond and femtosecond laser ablation processes rely on thermal or multiphoton ultrafast laser–matter interactions, respectively, the 405 nm laser ablation process could also rely on photochemical reactions. Consequently, the ablation characteristics, such as spot dimensions and material effects, may vary considerably between these different laser systems and wavelengths. Further comparative studies could provide deeper insights into the specific advantages and limitations of each ablation technique for applications in ophthalmology and other fields.

3.5. Characterization of Structural Modification and Chemical Composition

Following laser irradiation, the primary goal was to confirm that the physical and chemical properties of the IOLs are retained unaltered or at an acceptable degree, ensuring their suitability for ophthalmological use in patients. To verify this, micro-Raman measurements were conducted using the Ar⁺ 514.5 nm line for excitation. Care was taken to keep the laser power at a low level, to avoid laser-induced modifications: ca. 275 μW for the ×20 lens and 45 μW for the ×100 lens. Both regular and confocal micro-Raman spectra were acquired in the wavenumber region 100–3200 cm^{−1}. For the measurements with the ×20 lens, each spectrum corresponds to an acquisition time of 40 s for both IOLs, preceded by a bleaching time of 120 s: the reason for quenching the photoluminescence was to have an easier way to compare the Raman spectra of the polymer in the pristine and the laser-irradiated PMMA samples and thus detect possible irradiation-induced polymer modifications. To increase the possibility of probing a thinner surface layer of the sample, where the laser irradiation is expected to be maximal, with reduced interference from less irradiated areas lying deeper below the surface, we ran confocal measurements with the ×100 lens: the acquisition time was set at 40 s for PMMA IOLs and 120 s for acrylic IOLs without bleaching, so as to have a direct way to compare with results from the literature.

Raman spectra of the PMMA IOL before and after laser ablation with femtosecond 1064 nm and CW 405 nm are illustrated in Figure 11. The Raman spectra exhibit sharp peaks and broad bands, consistent with those reported in the literature [34–36]. Among the observed eight strongest Raman bands, the most prominent one is at 2951 cm^{−1}. This is assigned to the overlap of the symmetric C–H stretching vibration of O–CH₃ (methyl group forming part of the ether C–O–C chain) with the asymmetric C–H stretching vibration of α-CH₃ (methyl group attached to a backbone C) [35]. The corresponding symmetric

C–H stretching vibration of α -CH₃ is the shoulder seen at ca. 2885 cm⁻¹ (discernible only after sufficient magnification in the figure). The band at 3000 cm⁻¹ is the asymmetric C–H stretching vibration of O–CH₃. The 2843 cm⁻¹ is assigned to the CH₂ (methylene) symmetric C–H stretch; the CH₂ asymmetric C–H stretch is a shoulder at ca. 2935 cm⁻¹ (not discernible in the figure). The band at 1450 cm⁻¹ is the O–CH₃ symmetric bending vibration, while other-type methylene or methyl bending vibrations are seen at lower intensity in the vicinity, as shoulders or broader bands. The C=O stretch is observed at 1725 cm⁻¹, the C–O–C symmetric stretch appears at ca. 813 cm⁻¹, while the symmetric C–C–O (the central C is the one with the carboxyl bond) stretch is observed at 600 cm⁻¹ [34]. The symmetric CH₃ rocking modes form the doublet at 967 (α -CH₃) and 989 cm⁻¹ (O–CH₃).

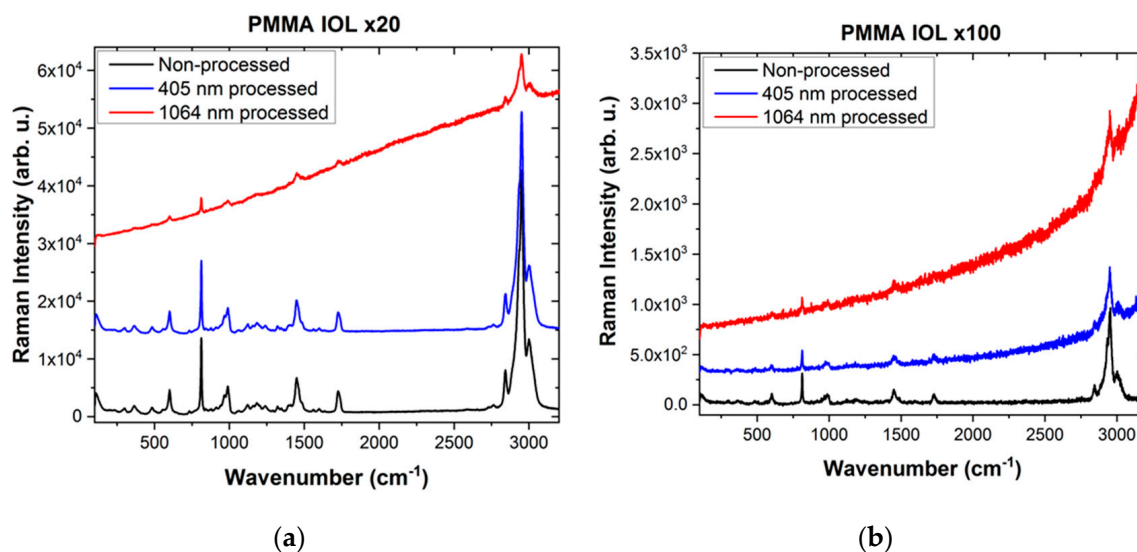


Figure 11. Raman spectra of PMMA IOLs before and after laser ablation with femtosecond 1064 nm and CW 405 nm lasers. (a) Regular; (b) confocal micro-Raman spectra.

In Figure 12, we present Raman spectra of the acrylic IOL before and after laser ablation with femtosecond 1064 nm and CW 405 nm. The pristine IOL Raman spectrum is very similar to the Alcon (Acrysof) model MA60BM IOL hydrophobic acrylic material (Alcon, Forth Wroth, TX, USA) shown in [37] or to the hydrophobic UV-photo-reactive polybenzylmethacrylate polymer (produced by Contateq, Eindhoven, The Netherlands) shown in [23] or even the copolymer-based Hydrophobic Foldable Ocular (HFO) material (produced by Soleko s.p.a.) reported in [38]. The spectra show narrow (compared to the PMMA spectrum) Raman bands in the 200–1650 cm⁻¹ range, the strongest of which are seen at 495, 621, 769, 825, 1002, 1031, 1202, 1303, 1417, 1446, 1584, and 1605 cm⁻¹ and are related to phenyl ring modes (621, 1002, 1031 cm⁻¹) [39] or C–C or C–O stretch or alkyl group deformation modes in the polymer substance. The two strong and broader bands in the region 2800–3200 cm⁻¹ with maximal intensities at 2923 cm⁻¹ and 3057 cm⁻¹ correspond to a convolution of CH₂ and CH₃ symmetric and asymmetric C–H stretching modes in singly and doubly bonded C atoms, respectively. The peak at approximately 1730 cm⁻¹ depicts the C=O stretching mode of acrylates, analogous with the 1725 cm⁻¹ mode for PMMA.

The absence of the C=C bond stretch signature at ca. 1640–50 cm⁻¹ in the pristine acrylic IOL material confirms the absence of residual monomers and its biocompatibility [37]. In the case of the PMMA IOL, a tiny component at ca. 1640 cm⁻¹ is hardly visible, revealing the presence of a low concentration of residual monomers.

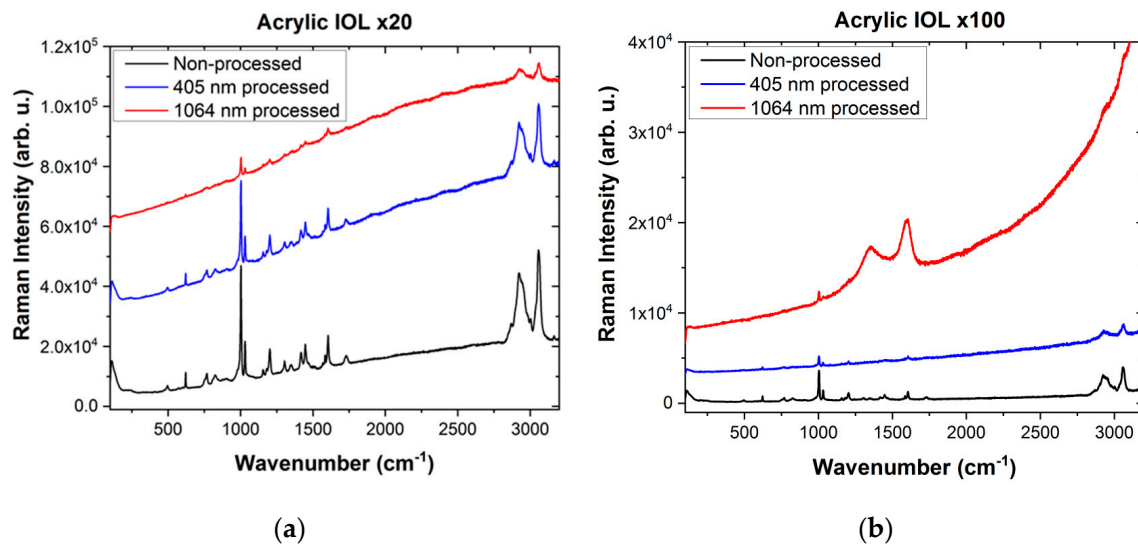


Figure 12. Raman spectra of acrylic IOLs before and after laser ablation with femtosecond 1064 nm and CW 405 nm lasers. (a) Regular; (b) confocal micro-Raman spectra.

The Raman spectra of areas structured with the CW 405 nm laser show a low Raman intensity diminution and a moderate background photoluminescence without significant changes in the band positions when compared with non-processed areas. This Raman intensity diminution indicates that, even though the polymer structure appears to remain almost unaltered, the ablation process must be producing some photo-thermal modification. These results are generally in line with other works on similar materials [23,40,41]. The Raman intensity diminution was stronger in the confocal spectra (acquired with the $\times 100$ lens); this indicates that, whatever the laser-irradiation-induced changes may be, they are localized closer to the surface, while the spectra acquired with the $\times 20$ lens correspond to a higher depth of field and consequently probe deeper in the material where the laser irradiation has not penetrated.

However, the laser-ablated areas structured with the femtosecond 1064 nm laser (0.8 μJ pulse energy, 100 kHz repetition rate) show a significant decrease in the intensity of the Raman peaks and a strong background photoluminescence. Defects, monomers, or other molecule fragments resulting from the degradation of the polymer network or backbone are at the origin of this background fluorescence either in the pyrolytic decomposition process or in the UV laser ablation process (see, e.g., [42]). A portion of this fluorescence may show up in the Raman spectra depending on which laser line is used for their acquisition. This observation is consistent with other studies [23], despite the different laser characteristics used in those studies (520 nm wavelength, 2 nJ pulse energy, and 63 MHz repetition rate) and even though the infrared 1064 nm irradiation photon energy is the lowest. Specifically, with confocal Raman (using the $\times 100$ lens), carbonization (see the disordered/amorphous-graphite-like doublet at 1351 and 1596 cm^{-1} [43], as in the case of above threshold irradiation of silicone-based hydrogel polymers [42]) is observed close to the surface layer for the acrylic material; this effect is not evident when the low magnification $\times 20$ lens is employed. The bands at 1305 and 1345 cm^{-1} do not show any broadening (at least as detected with the $\times 20$ lens). On the contrary, the broadening of the bands at 1310 and 1347 cm^{-1} in [23] has been interpreted as a laser-irradiation-induced photo-thermal damage and hence structural degradation of the acrylic IOL.

4. Discussion and Conclusions

This study presents a preliminary comparative analysis on the feasibility and efficacy of using direct laser-based micromachining technology with various characteristic lasers to modify IOLs' surfaces. The ultimate scope of this work is to be employed and optimized in future studies in order to achieve customizable vision correction solutions

based on relevant corneal wavefront data. The correction depth in customized IOL ranges typically from 0.2 μm to 3 μm , depending on the refractive error and the patients' visual correction preferences.

Our research revealed that infrared femtosecond 1064 nm laser ablation can produce 2D controlled patterns on PMMA IOLs within the range of a few micrometers and could be adapted to meet the required correction depths. Indeed, the micromachining process exhibited sensitivity to various laser parameters such as the repetition rate, pulse energy, and focus, affecting ablation depth and pattern uniformity, as observed with the acrylic IOL irradiation, thus providing the required flexibility. By considering the ablative laser modifications in relation to underlying thermal processes attributed to laser pulse cumulative heating, optimal laser operation regimes for the femtosecond laser were identified, providing improved micromachining performance compared to previous studies. More specifically, the employed Yb-based fiber laser at 1064 nm was operated at a 100 KHz repetition rate and thus adapted to heat diffusion time in polymer IOLs in order to eliminate heat accumulation during laser writing that could lead to discontinuous features as in previous studies.

Nanosecond 355 nm laser ablation effectively produced larger ablation areas, typically within the range of hundredths of micrometers, on acrylic IOLs and also exhibited sensitivity to exposure time, leading to variations in crater dimensions and structural changes within the IOLs. However, due to very low resolution and inadequate control in low-depth features (<2 μm), the nanosecond lasers cannot be considered as a good candidate for IOL patterning.

Our investigation with the CW 405 nm diode laser showcased its precision in modifying acrylic IOLs, despite the challenges in pattern generation due to exposure configuration and increased power requirements for PMMA IOLs. Notably, our study marks the first application of low-cost CW diode lasers for IOL surface modification, indicating promising prospects for laser ablation procedures in IOL customization.

Raman spectroscopy was extensively employed for the post-laser treatment characterization of structural integrity of the IOLs, for the case of femtosecond and CW diode laser patterning. Although typical micro-Raman did not identify significant structural changes, the application of confocal Raman spectroscopy, for the case of the femtosecond 1064 nm laser treatment of the acrylic lens, revealed the existence of relevant peaks attributed to amorphous carbon at the IOL surface layer only. However, this degradation needs to be further quantified and characterized in terms of the optical deterioration of IOL, in order to extract a safe conclusion on the effect of femtosecond laser patterning in functional characteristics of IOLs. On the other hand, no measurable degradation of IOLs was identified for diode laser patterning, suggesting another favorable characteristic for this patterning approach.

The differences observed in the outcomes of laser ablation between PMMA and acrylic IOLs can be attributed to variations in their material properties, including thermal conductivity, melting point, and absorption coefficients, among others. By systematically varying parameters such as laser energy, repetition rate, scanning speed, and focus position, the laser ablation process will be optimized for both IOLs under irradiation with different laser systems.

The roughness of femtosecond laser-induced micro-patterns can vary significantly with different laser powers. Higher laser power increases the energy delivered to the material, resulting in deeper ablation and potentially greater surface roughness due to more destructive material removal. For example, in a previous work [44], Ouyang et al. used for PMMA sample patterning a femtosecond laser at 1030 nm with a pulse duration of 240 fs and repetition rate of 610 kHz. It was found that at lower pulse energy (0.4 μJ) and a scanning speed of 1 mm/s, the patterning resulted in ripple-like microstructures. In contrast, higher pulse energies (0.8 μJ and 1.2 μJ) at the same speed led to the formation of bumps and pores. Increasing the scanning speeds to 2 mm/s and 8 mm/s reduced the groove width but increased surface roughness due to the presence of microparticles. These

effects are also observed at high repetition rates and low scanning speeds, where the pulse energy is much higher than the ablation threshold, leading to significant heat accumulation. Therefore, as demonstrated in our work, a careful selection of writing parameters is needed for efficient patterning with reduced roughness. Furthermore, it could be noted that in the same aforementioned work, smoothing of femtosecond laser-machined PMMA surfaces was attempted by thermal annealing treatment at 160 °C for various time intervals, thus considerably improving the roughness. Although this technique was not investigated in PMMA or acrylic IOLs in our work, it could be considered in future studies provided that IOLs can withstand such a thermal annealing process.

Each laser system has its unique interaction mechanism with the target material, and selecting the most appropriate one based on the desired outcome is crucial. Specifically with femtosecond lasers, we leverage multiphoton absorption, enabling us to pattern materials that do not readily absorb at the laser's wavelength. However, both PMMA and acrylic IOLs exhibit significant absorption in the 355 nm (nanosecond laser) and 405 nm (diode laser) ranges and although this enhances the efficiency of the inscription process at the surface, adaptive focusing is required for patterning beneath the material's surface and at various depths, making the process quite challenging. Another technical issue to address in future studies is the challenge of maintaining and accurately controlling the required focus during the laser writing process on the curved surfaces of IOLs. The inclusion of rotational translation stages in the micromachining station, along with a dynamic autofocus system, will significantly enhance the precision and accuracy of IOL patterning.

Further exhaustive studies are required for the development of accurate IOL patterning approaches, based on the current findings, that would be compatible with IOL surface tailoring based on corneal wavefront data, enabling personalized vision correction solutions and enhancing patient outcomes in cataract surgery.

Author Contributions: Conceptualization, C.B., M.K. and C.R.; methodology, M.K. and C.R.; validation, M.K., C.R., A.S. and C.B.; formal analysis, A.S., D.P., C.R., M.K. and D.M.; resources, D.M. and D.P.; investigation, A.S., D.P., C.R., M.K., C.B. and D.M.; writing—original draft preparation, A.S., D.P., C.R. and M.K.; writing—review and editing, A.S., M.K., D.P., C.B., D.M. and C.R.; supervision, M.K. and C.R.; project administration, M.K. and C.R.; funding acquisition, M.K. and C.R. All authors have read and agreed to the published version of the manuscript.

Funding: This research work was supported by the Hellenic Foundation for Research and Innovation (H.F.R.I.) under the “First Call for H.F.R.I. Research Projects to support Faculty members and Researchers and the procurement of high-cost research equipment grant” (Project Number: HFRI-FM17-640, InPhoQuC).

Institutional Review Board Statement: Not applicable.

Informed Consent Statement: Not applicable.

Data Availability Statement: The original contributions presented in the study are included in the article; further inquiries can be directed to the corresponding author.

Acknowledgments: E. Angelakos of the SME company Opticon ABEE (Greece) is gratefully acknowledged for providing access to the CW diode laser micromachining setup, in the frame of an exclusive research collaboration with NHRF. N. Diamantopoulou is acknowledged for providing technical help at the preliminary stage of this research.

Conflicts of Interest: The authors declare no conflicts of interest.

References

1. Bloemendal, H.; De Jong, W.; Jaenicke, R.; Lubsen, N.H.; Slingsby, C.; Tardieu, A. Ageing and Vision: Structure, Stability and Function of Lens Crystallins. *Prog. Biophys. Mol. Biol.* **2004**, *86*, 407–485. [[CrossRef](#)] [[PubMed](#)]
2. Vacalebri, M.; Frison, R.; Corsaro, C.; Neri, F.; Santoro, A.; Conoci, S.; Anastasi, E.; Curatolo, M.C.; Fazio, E. Current State of the Art and Next Generation of Materials for a Customized IntraOcular Lens According to a Patient-Specific Eye Power. *Polymers* **2023**, *15*, 1590. [[CrossRef](#)] [[PubMed](#)]

3. Luo, C.; Wang, H.; Chen, X.; Xu, J.; Yin, H.; Yao, K. Recent Advances of Intraocular Lens Materials and Surface Modification in Cataract Surgery. *Front. Bioeng. Biotechnol.* **2022**, *10*, 913383. [[CrossRef](#)] [[PubMed](#)]
4. Han, Y.; Tang, J.; Xia, J.; Wang, R.; Qin, C.; Liu, S.; Zhao, X.; Chen, H.; Lin, Q. Anti-Adhesive and Antiproliferative Synergistic Surface Modification of Intraocular Lens for Reduced Posterior Capsular Opacification. *Int. J. Nanomed.* **2019**, *14*, 9047–9061. [[CrossRef](#)]
5. Bozukova, D.; Pagnoulle, C.; De Pauw-Gillet, M.-C.; Desbief, S.; Lazzaroni, R.; Ruth, N.; Jérôme, R.; Jérôme, C. Improved Performances of Intraocular Lenses by Poly(Ethylene Glycol) Chemical Coatings. *Biomacromolecules* **2007**, *8*, 2379–2387. [[CrossRef](#)] [[PubMed](#)]
6. Wilkins, M.R.; Allan, B.; Rubin, G. Moorfields IOL Study Group Spectacle Use after Routine Cataract Surgery. *Br. J. Ophthalmol.* **2009**, *93*, 1307–1312. [[CrossRef](#)] [[PubMed](#)]
7. Wang, S.Y.; Stem, M.S.; Oren, G.; Shtein, R.; Lichter, P.R. Patient-Centered and Visual Quality Outcomes of Premium Cataract Surgery: A Systematic Review. *Eur. J. Ophthalmol.* **2017**, *27*, 387–401. [[CrossRef](#)] [[PubMed](#)]
8. Ruhswurm, I.; Scholz, U.; Zehetmayer, M.; Hanselmayer, G.; Vass, C.; Skorpik, C. Astigmatism Correction with a Foldable Toric Intraocular Lens in Cataract Patients. *J. Cataract. Refract. Surg.* **2000**, *26*, 1022–1027. [[CrossRef](#)] [[PubMed](#)]
9. Alio, J.L.; Plaza-Puche, A.B.; Fernández-Buenaga, R.; Pikkell, J.; Maldonado, M. Multifocal Intraocular Lenses: An Overview. *Surv. Ophthalmol.* **2017**, *62*, 611–634. [[CrossRef](#)]
10. Aslam, T.M.; Devlin, H.; Dhillon, B. Use of Nd:YAG Laser Capsulotomy. *Surv. Ophthalmol.* **2003**, *48*, 594–612. [[CrossRef](#)]
11. Schriebl, S.M.; Menapace, R.; Stifter, E.; Zaruba, D.; Leydolt, C. Posterior Capsule Opacification and Neodymium:YAG Laser Capsulotomy Rates with 2 Microincision Intraocular Lenses: Four-Year Results. *J. Cataract. Refract. Surg.* **2015**, *41*, 956–963. [[CrossRef](#)] [[PubMed](#)]
12. Seo, Y.; Kim, S.; Lee, H.S.; Park, J.; Lee, K.; Jun, I.; Seo, H.; Kim, Y.J.; Yoo, Y.; Choi, B.C.; et al. Femtosecond Laser Induced Nano-Textured Micropatterning to Regulate Cell Functions on Implanted Biomaterials. *Acta Biomater.* **2020**, *116*, 138–148. [[CrossRef](#)] [[PubMed](#)]
13. Madrid-Costa, D.; Pérez-Vives, C.; Ruiz-Alcocer, J.; Albarrán-Diego, C.; Montés-Micó, R. Visual Simulation through Different Intraocular Lenses in Patients with Previous Myopic Corneal Ablation Using Adaptive Optics: Effect of Tilt and Decentration. *J. Cataract. Refract. Surg.* **2012**, *38*, 774–786. [[CrossRef](#)] [[PubMed](#)]
14. Kalli, K.; Riziotis, C.; Posporis, A.; Markos, C.; Koutsides, C.; Ambran, S.; Webb, A.S.; Holmes, C.; Gates, J.C.; Sahu, J.K.; et al. Flat Fibre and Femtosecond Laser Technology as a Novel Photonic Integration Platform for Optofluidic Based Biosensing Devices and Lab-on-Chip Applications: Current Results and Future Perspectives. *Sens. Actuators B Chem.* **2015**, *209*, 1030–1040. [[CrossRef](#)]
15. Athanasekos, L.; Vasileiadis, M.; El Sachat, A.; Vainos, N.A.; Riziotis, C. ArF Excimer Laser Microprocessing of Polymer Optical Fibers for Photonic Sensor Applications. *J. Opt.* **2015**, *17*, 015402. [[CrossRef](#)]
16. Koo, J.-S.; Smith, P.G.R.; Williams, R.B.; Riziotis, C.; Grossel, M.C. UV Written Waveguides Using Crosslinkable PMMA-Based Copolymers. *Opt. Mater.* **2003**, *23*, 583–592. [[CrossRef](#)]
17. Sinani, A.; Karachousos-Spiliotakopoulos, K.; Tangoulis, V.; Manouras, T.; Angelakos, E.; Riziotis, C. Sub-Diffraction Limited Direct Diode Laser Patterning of Methacrylic Polymer Thin Films Doped with Silver Nanoparticles. In Proceedings of the Laser-based Micro- and Nanoprocessing XVIII, San Francisco, CA, USA, 29 January–1 February 2024; Kling, R., Pflöging, W., Sugioka, K., Eds.; SPIE: San Francisco, CA, USA, 2024; p. 44.
18. Phillips, K.C.; Gandhi, H.H.; Mazur, E.; Sundaram, S.K. Ultrafast Laser Processing of Materials: A Review. *Adv. Opt. Photon.* **2015**, *7*, 684. [[CrossRef](#)]
19. Rauh, S.; Wöbbing, K.; Li, M.; Schade, W.; Hübner, E.G. From Femtosecond to Nanosecond Laser Microstructuring of Conical Aluminum Surfaces by Reactive Gas Assisted Laser Ablation. *ChemPhysChem* **2020**, *21*, 1644–1652. [[CrossRef](#)]
20. Krüger, J.; Martin, S.; Mädebach, H.; Urech, L.; Lippert, T.; Wokaun, A.; Kautek, W. Femto- and Nanosecond Laser Treatment of Doped Polymethylmethacrylate. *Appl. Surf. Sci.* **2005**, *247*, 406–411. [[CrossRef](#)]
21. Kanidi, M.; Papadimitropoulou, A.; Charalampous, C.; Chakim, Z.; Tsekenis, G.; Sinani, A.; Riziotis, C.; Kandyła, M. Regulating MDA-MB-231 Breast Cancer Cell Adhesion on Laser-Patterned Surfaces with Micro- and Nanotopography. *Biointerphases* **2022**, *17*, 021002. [[CrossRef](#)]
22. Serafetinides, A.A.; Makropoulou, M.; Fabrikesi, E.; Spyratou, E.; Bacharis, C.; Thomson, R.R.; Kar, A.K. Ultrashort Laser Ablation of PMMA and Intraocular Lenses. *Appl. Phys. A* **2008**, *93*, 111–116. [[CrossRef](#)]
23. Sola, D.; Cases, R. High-Repetition-Rate Femtosecond Laser Processing of Acrylic Intra-Ocular Lenses. *Polymers* **2020**, *12*, 242. [[CrossRef](#)] [[PubMed](#)]
24. Sola, D.; Aldana, J.R.V.D.; Artal, P. The Role of Thermal Accumulation on the Fabrication of Diffraction Gratings in Ophthalmic PHEMA by Ultrashort Laser Direct Writing. *Polymers* **2020**, *12*, 2965. [[CrossRef](#)] [[PubMed](#)]
25. De Marco, C.; Eaton, S.M.; Suriano, R.; Turri, S.; Levi, M.; Ramponi, R.; Cerullo, G.; Osellame, R. Surface Properties of Femtosecond Laser Ablated PMMA. *ACS Appl. Mater. Interfaces* **2010**, *2*, 2377–2384. [[CrossRef](#)] [[PubMed](#)]
26. Baset, F.; Villafranca, A.; Guay, J.-M.; Bhardwaj, R. Femtosecond Laser Induced Porosity in Poly-Methyl Methacrylate. *Appl. Surf. Sci.* **2013**, *282*, 729–734. [[CrossRef](#)]
27. Eaton, S.M.; Zhang, H.; Herman, P.R.; Yoshino, F.; Shah, L.; Bovatsek, J.; Arai, A.Y. Heat Accumulation Effects in Femtosecond Laser-Written Waveguides with Variable Repetition Rate. *Opt. Express* **2005**, *13*, 4708. [[CrossRef](#)] [[PubMed](#)]

28. Della Valle, G.; Osellame, R.; Laporta, P. Micromachining of Photonic Devices by Femtosecond Laser Pulses. *J. Opt. A Pure Appl. Opt.* **2009**, *11*, 013001. [[CrossRef](#)]
29. Agari, Y.; Ueda, A.; Omura, Y.; Nagai, S. Thermal Diffusivity and Conductivity of PMMA/PC Blends. *Polymer* **1997**, *38*, 801–807. [[CrossRef](#)]
30. Day, D.; Gu, M. Microchannel Fabrication in PMMA Based on Localized Heating by Nanojoule High Repetition Rate Femtosecond Pulses. *Opt. Express* **2005**, *13*, 5939. [[CrossRef](#)]
31. Hofmeister, A.; Whittington, A. Thermal Diffusivity and Conductivity of Glasses and Melts. In *Encyclopedia of Glass Science, Technology, History, and Culture*; Richet, P., Conradt, R., Takada, A., Dyon, J., Eds.; Wiley: Hoboken, NJ, USA, 2021; pp. 487–500, ISBN 978-1-118-79942-0.
32. Kanidi, M.; Dagkli, A.; Kelaidis, N.; Palles, D.; Aministragia-Giamini, S.; Marquez-Velasco, J.; Colli, A.; Dimoulas, A.; Lidorikis, E.; Kandyla, M.; et al. Surface-Enhanced Raman Spectroscopy of Graphene Integrated in Plasmonic Silicon Platforms with Three-Dimensional Nanotopography. *J. Phys. Chem. C* **2019**, *123*, 3076–3087. [[CrossRef](#)]
33. Kotsifaki, D.G.; Kandyla, M.; Lagoudakis, P.G. Near-Field Enhanced Optical Tweezers Utilizing Femtosecond-Laser Nanostructured Substrates. *Appl. Phys. Lett.* **2015**, *107*, 211111. [[CrossRef](#)]
34. Willis, H.A.; Zichy, V.J.I.; Hendra, P.J. The Laser-Raman and Infra-Red Spectra of Poly(Methyl Methacrylate). *Polymer* **1969**, *10*, 737–746. [[CrossRef](#)]
35. Dybal, J.; Krimm, S. Normal-Mode Analysis of Infrared and Raman Spectra of Crystalline Isotactic Poly(Methyl Methacrylate). *Macromolecules* **1990**, *23*, 1301–1308. [[CrossRef](#)]
36. Chaurasia, S.; Rao, U.; Mishra, A.K.; Sijoy, C.D.; Mishra, V. Raman Spectroscopy of Poly (Methyl Methacrylate) under Laser Shock and Static Compression. *J. Raman Spectrosc.* **2020**, *51*, 860–870. [[CrossRef](#)]
37. Jung, G.B.; Jin, K.-H.; Park, H.-K. Physicochemical and Surface Properties of Acrylic Intraocular Lenses and Their Clinical Significance. *J. Pharm. Investig.* **2017**, *47*, 453–460. [[CrossRef](#)]
38. Rusciano, G.; Capaccio, A.; Pesce, G.; Sasso, A. Experimental Study of the Mechanisms Leading to the Formation of Glistenings in Intraocular Lenses by Raman Spectroscopy. *Biomed. Opt. Express* **2019**, *10*, 1870. [[CrossRef](#)] [[PubMed](#)]
39. Liu, H.H.; Lin, S.H.; Yu, N.T. Resonance Raman Enhancement of Phenyl Ring Vibrational Modes in Phenyl Iron Complex of Myoglobin. *Biophys. J.* **1990**, *57*, 851–856. [[CrossRef](#)]
40. Jia, W.; Luo, Y.; Yu, J.; Liu, B.; Hu, M.; Chai, L.; Wang, C. Effects of High-Repetition-Rate Femtosecond Laser Micromachining on the Physical and Chemical Properties of Polylactide (PLA). *Opt. Express* **2015**, *23*, 26932. [[CrossRef](#)]
41. Sola, D.; Milles, S.; Lasagni, A.F. Direct Laser Interference Patterning of Diffraction Gratings in Safrofilcon-A Hydrogel: Fabrication and Hydration Assessment. *Polymers* **2021**, *13*, 679. [[CrossRef](#)]
42. Ding, L.; Cancado, L.G.; Novotny, L.; Knox, W.H.; Anderson, N.; Jani, D.; Linhardt, J.; Blackwell, R.I.; Künzler, J.F. Micro-Raman Spectroscopy of Refractive Index Microstructures in Silicone-Based Hydrogel Polymers Created by High-Repetition-Rate Femtosecond Laser Micromachining. *J. Opt. Soc. Am. B* **2009**, *26*, 595. [[CrossRef](#)]
43. Ferrari, A.C.; Robertson, J. Interpretation of Raman Spectra of Disordered and Amorphous Carbon. *Phys. Rev. B* **2000**, *61*, 14095–14107. [[CrossRef](#)]
44. Ouyang, Z.; Long, J.; Wu, J.; Lin, J.; Xie, X.; Tan, G.; Yi, X. Preparation of High-Quality Three-Dimensional Microstructures on Polymethyl Methacrylate Surfaces by Femtosecond Laser Micromachining and Thermal-Induced Micro-Leveling. *Opt. Laser Technol.* **2022**, *145*, 107499. [[CrossRef](#)]

Disclaimer/Publisher’s Note: The statements, opinions and data contained in all publications are solely those of the individual author(s) and contributor(s) and not of MDPI and/or the editor(s). MDPI and/or the editor(s) disclaim responsibility for any injury to people or property resulting from any ideas, methods, instructions or products referred to in the content.